



Prediction of the deformation and local buckling behavior of structural systems using the deep neural network direct stiffness method (DNN-DSM)

Andreas Müller¹, Andreas Taras²

Abstract

This paper presents a novel approach to carrying out a beam-element analysis that accounts for the nonlinear deformation behavior of various RHS and SHS sections, ranging from mild to high-strength steel prefabricated by hot-rolling or cold forming. The deep neural network direct stiffness method (DNN-DSM), which makes use of deep neural networks (DNN), a subgroup of machine learning algorithms and more general artificial intelligence approaches, is used to predict the nonlinear stiffness matrix terms in a beam-element formulation for the implementation in the direct stiffness matrix (DSM). Those predictions are made by trained DNN models resulting from an extensive pool of geometrically material nonlinear simulations with additional imperfections (GMNIA) using shell based models. First implementations of this method are able to accurately predict the nonlinear load-displacement and moment-rotation behavior of various sections with great accuracy, combining the precision of shell analysis and the computational efficiency of beam element analysis. Previous published investigations already showed the feasibility and advantages of this method but were restricted to the small-scale prediction of the local buckling. This paper will go one step further and apply the DNN-DSM method to members, more specifically to columns and beams dominated either by normal forces or bending, accompanied by comparisons with equivalent Abaqus models.

1. Introduction and Motivation

1.1 Problem Definition

The hypothetical possibility of accounting for plastic distribution in structural design was first suggested by Ewing (Ewing 1899), although remaining only a theoretical approach due to the lack of physical tests and computational recourses. From the beginning of the 20th century research investigations focused on the advanced plastic analysis of steel structures, in particular members and frames, recognizing its potential in plastic redistributions (Meyer 1908, Kazinczy 1914, Kist 1920, Gruning 1926, Maier-Leibnitz 1928, Maier-Leibnitz 1929, Fritsche 1930, Schaim 1930, Girkmann 1931, Baker 1938, Baker and Roderick 1940, Baker et al. 1956, Massonnet 1976, Driscoll et al. 1965, Galambos 1968). As a result of these investigations, questions regarding available rotation capacities arose, leading to the known concept of cross-section classifications along with

¹ PhD Student, Steel and Composite Structures, ETH Zurich <andreas.mueller@ibk.baug.ethz.ch>

² Professor, [Chair of](#) Steel and Composite Structures, ETH Zurich <taras@ibk.baug.ethz.ch>

practice-oriented simplifications; all assumptions go back to a time period where the main goal was a practically suited development of analytical approximations suited for hand calculations. Nowadays, code provisions (EN 1993-1-1 2006, AISC 360-16 2016) still incorporate these assumptions, leading to conservative design conclusions, especially for materials with pronounced hardening capacities and higher strength steel grades. The traditional separation of analysis and verification, whereby both are dependent on the cross-sectional slenderness and corresponding classification into categories ranging from stocky to slender, affects high strength steel (HSS) sections in particular. These often would need to be classified as slender cross-sections, forcing designers to forego all plastic redistribution even when this is in fact not fully justified, typically using design rules with effective widths in accordance to standards such as Eurocode 3 (EN 1993-1-5:2006) or comparable international codes. Available deformation capacities (Toffolon et.al. 2019a, Toffolon et.al. 2019b, Toffolon and Taras 2019c, Toffolon and Taras 2019d, Meng et.al. 2019, Müller and Taras 2019), different material properties between hot rolled and cold-formed structural profiles (EN 10210-2 2006; EN 10219-2 2006) including strain hardening and more precise material laws, proposed by (Yun and Gardner 2017, Yun and Gardner 2018) are generally neglected in these traditional approaches.

Advanced nonlinear analysis methods with shell finite elements, so called GMNIA simulations (**g**eometrically **m**aterial **n**onlinear **a**nalysis with **i**mperfections) are capable of accounting for those positive effects. Nevertheless, being computationally time intensive and complex these methods remain not suitable for the use in practice at its current point. Approaches, which combine the efficiency of beam finite elements and the ability to account for slenderness-dependent deformation capacities and nonlinear redistribution are being developed within the CSM (Gardner 2008, Fieber 2019, Walport 2019) for different materials.

This paper presents the initial steps that were taken to develop a novel approach to carry out a beam-element analysis that accounts for the nonlinear load-displacement behaviour of hot rolled and cold-formed SHS and RHS sections (DIN EN 10210-2 2006, DIN EN 10219-2 2006) of different local slenderness. It build up on investigations discussed in (Müller and Taras 2022 a), Müller and Taras 2022 b), Müller and Taras 2022 c)) and presents initial steps towards its implementation within the DSM framework, as well as first results with exemplary comparisons with shell finite element results and experiments.

1.2 Proposed Method

Fig 1 a) shows the general implementation within the elastic DSM formulation using the example of a truss frame, dominated by normal forces. An isolated beam element represented by the local elastic stiffness matrix K_{local} is constructed, assembled to a global system of equations and solved by calculating the inverse global stiffness matrix and subsequently the associated displacements U_{sys} . Here only the terms dominated by the normal force are highlighted in red, since the first implementation steps presented within this paper will focus exclusively on this load case. The novel method denominated as DNN-DSM (deep neural network direct stiffness method) makes use of machine and deep learning techniques (ML and DL) to predict the nonlinear stiffness matrix of a beam element under different deformations and rotations acting in plane.

A general overview, starting with data development up to the method Implementation, is presented within Fig. 1 b). The developed deep neural network (DNN) models are based on data sets derived

from a pool of numerical (LBA and GMNIA) shell elements simulations, designed in such a way that only local buckling is the driving instability phenomena for the investigated cross-sections (s. Sec. 2.1). Therefore, the local length of the elements was set to the maximum of whether the height or the width of the cross-section. This assumption was made within a first feasibility study. Thorough investigations on cross-section and load dependent buckling lengths are under way, following up the research carried out by (Fieber 2019). The extracted data includes geometrical and mechanical parameters based on (DIN EN 10210-2 2006, DIN EN 10219-2 2006) as well as directly simulation related outputs including the cross-section dependent displacement u and the tangent stiffness K_T . Subsequently, the resulting database is used for the training of the DNN models, with the tangent stiffness as the governing output parameter (s. Sec. 2.2). The DNN based prediction of the tangent stiffness $K_{DNN,local}$ is thereby evaluated for every discretized beam element within a global structure, assembled to a global stiffness matrix $K_{DNN,sys}$ and used to evaluate a differential force ΔF_{sys} , which is calculated under the consideration of incremental displacement steps ΔU_{sys} .

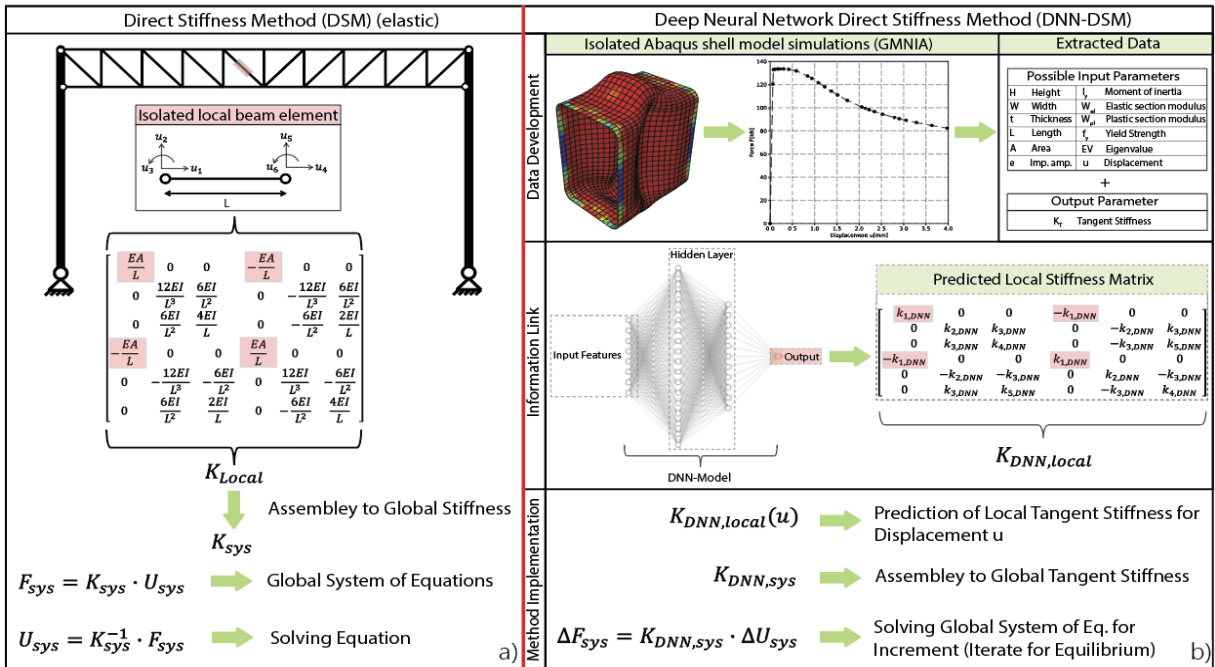


Figure 1: a) Direct Stiffness Method (elastic formulation), b) Initial formulation of the Deep Neural Network Direct Stiffness Method (DNN-DSM), published in (Müller and Taras 2022a), Müller and Taras, 2022b)

2. Finite Element Model Assumptions

The developed Abaqus models make use of iso-parametric shell elements with reduced integration (type S4R in Abaqus), with a mesh density of around 60 elements in circumferential and (depending on the total member length) 50 – 100 elements per meter in longitudinal direction. The geometry of the profiles is based on European standards (EN 10210-2:2006, EN 10219-2:2006) with a local length L (longitudinal direction) set as the bigger value of either the width W or the height H of the cross-section. Therefore, the loads and deformations are applied through defined reference points (RF-Points) which are located at the upper and lower edge of the cross-section (s. Fig. 2).

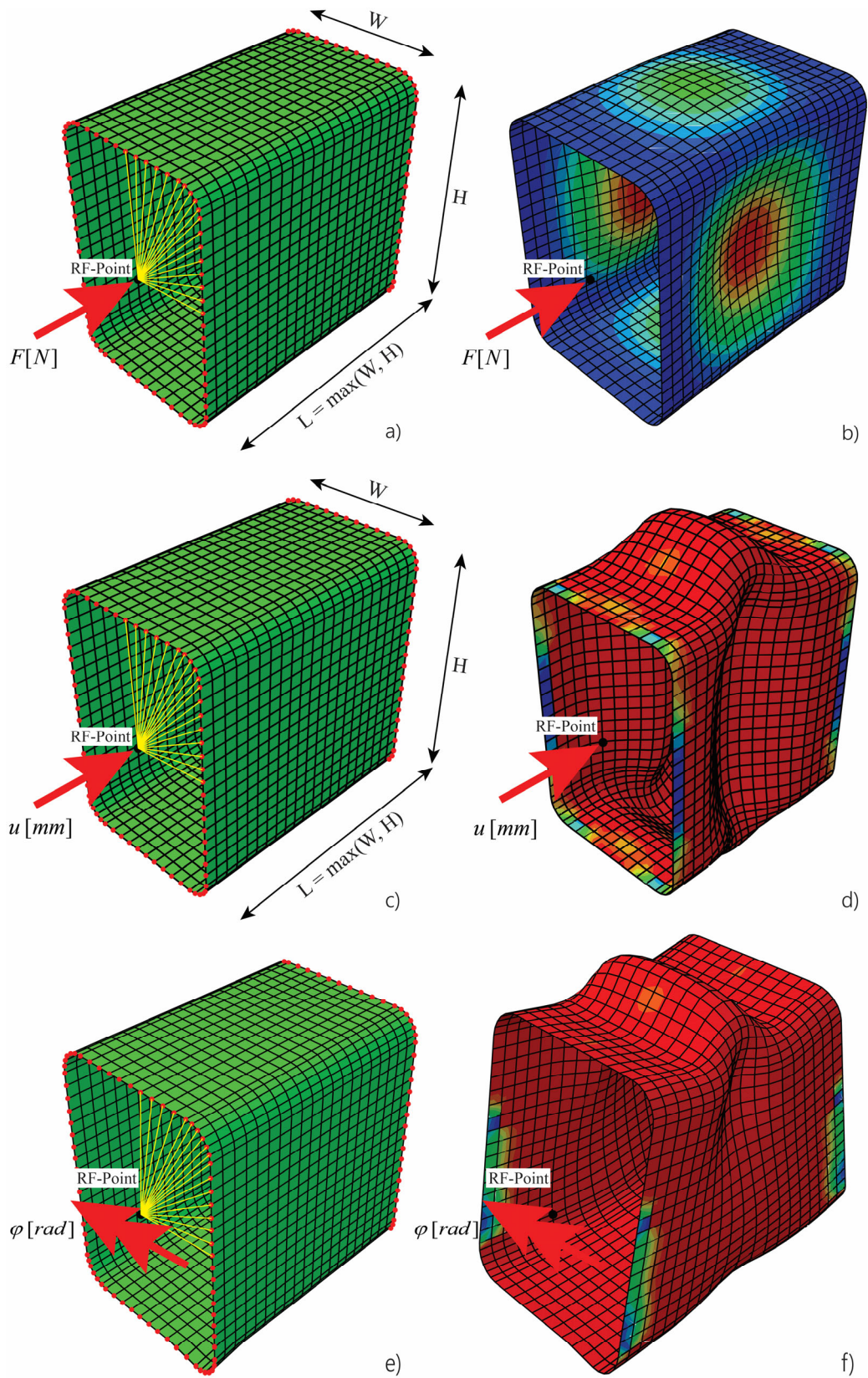


Figure 2: a) Finite element model of an RHS section; b) Deformation in the direction of the longitudinal axis

These are connected through multi-point constraints (MPC-Beam formulation) to associated node sets along the upper and lower profile outer edge (s. Fig. 2 a) shown exemplary for the quarter range of the cross-section). This definition implies a rigid connection between the nodes at the extremity and a reference node at the centroid of the respective sections. All boundary conditions were set as fixed, except for the deformation in the longitudinal direction. For the purposes of this study, an elastic-ideal plastic material model was used, with an infinite yield plateau assumed at a stress level $\sigma_{\text{von-Mises}} = f_y$, without an explicit consideration of residual stresses within the Abaqus models. The validation of the Abaqus model is based on an extensive analytical, numerical and experimental campaign, conducted by the authors and other researchers between the years of 2017 and 2019 at the University of Bundeswehr Munich, in the context of the EU-funded (RFCFS) project HOLLOSSTAB (Grand Nr. 2015-709892). The reader is referred to the references of the project for further details in (Toffolon et.al. 2019a, Toffolon et.al. 2019b, Toffolon and Taras 2019c, Toffolon and Taras 2019d, Meng et.al. 2019).

The simulation process for the generation of the required data sets is always performed in two steps. In a first step an LBA analysis is carried out in order to identify the elastic critical buckling resistance of the cross-section and the eigenmode shape as the critical imperfection form. In a second step, a GMNIA simulation is performed to determine an elasto-plastic buckling load – the realistic buckling resistance that considers both material and geometric nonlinearities – of the cross-section as well as the courses of the pre- and post-buckling range. The nonlinear calculations in Abaqus were performed using the static general stress analysis.

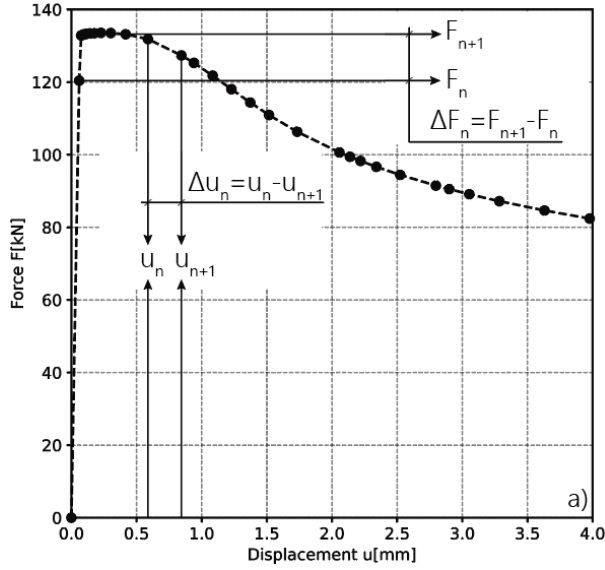
3. Data Development

The developed data sets for the SHS and RHS profiles are chosen taking into account parameters found in EN 10210-2:2 2006 and EN 10219-2:2006 for hot-finished respectively cold-formed structural hollow sections. A total of 361 European profile shapes was taken into account. All additional properties for this study are summarized in Tab. 1. This parameters form the basis for further LBA and GMNIA simulations conducted in Abaqus (Abaqus, 2016).

Table 1: Investigated profiles (DIN EN 10210-2 2006, DIN EN 10219-2 2006) and applied parameters

Used Profiles	Number of Sections	Dimension Range c/t
SHS hot rolled	88	8.0 – 47.62
SHS cold-formed	88	8.0 – 47.62
RHS hot rolled	93	9.52 – 56.25
RHS cold-formed	92	12.5 – 55.55
Used Parameters	Number of Parameters	Values
Steel grade f_y	3	S355, S460, S700
Imperfection amplitude e_0	3	B/200, B/300, B/400

The parameters from Tab.1 led to a total amount of 361 LBA and 6492 GMNIA simulations for the load case of pure compression N and pure bending M. This data basis is subsequently used for the extraction of the input features used for the training of the DNN models. Therefore, the LBA analysis output from Abaqus was used to extract the cross-section dependent elastic critical buckling load. The GMNIA analysis results, on the other hand, were used to determine the incremental deformation steps Δu_n and an associated differential force ΔF_n , see Fig. 3 a).



H	Height	I_y	Moment of inertia
W	Width	W_{el}	Elastic section modulus
t	Thickness	W_{pl}	Plastic section modulus
L	Length	f_y	Yield Strength
A	Area	EV	Eigenvalue
e	Imperfection amp.	K_T	Tangent Stiffness
u	Displacement		

SHS-Profiles

Hot rolled
DIN EN 10210-2 (2006)
and
Cold-formed
DIN EN 10219-2 (2006)

RHS-Profiles

Hot rolled
DIN EN 10210-2 (2006)
and
Cold-formed
DIN EN 10219-2 (2006)

Figure 3: a) Data extraction from Abaqus simulations, b) Overview of selected features

These values were subsequently used to calculate an incremental tangent stiffness $K_{T,n}$, for the entire displacement and rotation range of a cross-section in the pre- and post-buckling range. See Eq.(1) for the load case of pure compression.

$$K_{T,n} = \frac{\Delta F_n}{\Delta u_n} \quad (1)$$

4. DNN Model Development and Results

4.1 Preface to Deep Neural Networks

A common representation of an artificial neuron (Frochte 2018) can be written as follows with Eq.(2). The optimization process in a neural network uses backpropagation as a technique to update the weights within a training procedure.

$$y(x) = a \cdot \left(\left(\sum W_n \cdot x_n \right) + b \right) \quad (2)$$

It consists mainly of three parameters, (i) the weights W , which are updated during the training of the DNN model throughout a preset amount of epochs (optimization steps), (ii) a bias b as an additional trainable nonzero value which is added to the summation of weighted inputs of a neuron, (iii) a represents the activation function, with an inherent predefined threshold. Throughout the presented investigations the ReLU function from Eq.(3) was used.

$$\text{ReLU} : f(x) = \max \begin{cases} 0, & x < 0 \\ x, & x \geq 0 \end{cases} \quad (3)$$

The overall estimated accuracy of a neural network is highly dependent on the quality and distribution of the input parameters. In many cases it is therefore necessary to transform or scale these

values, using different methods like normalization (s. Eq.(4)) or standardization (s. Eq.(5)) as follows (Frochte 2018). Data transformation eliminates the major problem of multiple features having different magnitudes, ranges and units by scaling them down. Therefore, data normalization is used to scale the magnitudes of available features between the values of 0 and 1 (or -1 and 1), corresponding to the lowest and highest values. Standardizing the data means rescaling it, while the mean value is set to 0 and the standard deviation to 1. In a lot of engineering applications data standardization shows better performance evaluations, since outliers are taken better into account.

$$\hat{x}^{(i)} = \frac{x^{(i)} - x_{\min}^{(i)}}{x_{\max}^{(i)} - x_{\min}^{(i)}} \quad (4)$$

$$\bar{x}^{(i)} = \frac{x^{(i)} - \bar{x}^{(i)}}{\sigma} \quad (5)$$

with:

$\bar{x}^{(i)}$ Mean value of an input feature
 σ Standard deviation of an input feature

$$r^2 = 1 - \frac{\sum_{i=1}^n (y_i - \hat{y}_i)^2}{\sum_{i=1}^n (y_i - \bar{y}_i)^2} \quad (6)$$

with:

$y_i, \hat{y}_i, \bar{y}_i$ Actual output, predicted output, standard deviation

The model accuracy is measured by using the r^2 value from Eq.(6), a common metric for regression problems.

4.2 Preliminary Investigations and Conclusions

Preliminary investigations involved the assessment of the data, i.e. its distribution and the influence on the performance, predictions in the pre- and post-buckling range, dimensions of the input and output parameters, as well as the feature importance. This investigations are presented in more detail in (Müller and Taras 2022 a), Müller and Taras 2022 b), Müller and Taras 2022 c)) and can be summarized as follows:

- i. The raw data extracted from Abaqus needs to be artificially extended in the elastic range. This can be attributed to a large initial step size in the GMNIA calculations, which was chosen in the solver settings to minimize the computational effort.
- ii. It was obtained that a splitting between hot rolled and cold-formed SHS and RHS profiles and the pre- and post-buckling range led to a significantly better performance of the DNN models.

- iii. The input features were standardized using Eq.(5). The output, i.e. the predicted values were normalized by the elastic stiffness K_T/K_e .
- iv. Feature importance investigations were evaluated with decision tree-based algorithms. Two methodologies (Random Forest Regressor (Breiman 2001) and XGBoost Regressor (Chen and Guestrin 2016)) proved to be successful in the case of the present data sets.

5.3 DNN Architecture and Hyperparameters

The used hyperparameters for the training of the DNN models are summarized within Tab. 2. A total of 193 individual combinations was tested within the framework of preliminary investigations using the Random Search Method. this workflow is suitable in order to detect the overall tendencies within the DNN architecture. All calculations were performed on the basis of a train and test philosophy, meaning that a specific data amount was used for the training (80%) and an additional independent amount for the validation process (20%).

Table 2: Estimated hyperparameters

Model Parameters	Selection
Hidden layer 1 (neurons)	27
Hidden layer 2 (neurons)	27
Hidden layer 3 (neurons)	18
Hidden layer 4 (neurons)	9
Activation function	ReLU
Optimizer	Adam
Learning rate	0.0005

Fig. 4 presents some of the results, estimated from the DNN model for hot-rolled RHS and SHS profiles in the pre-buckling range. The x-axis represented the simulated values and the y-axis the predicted values. Fig. 4 a) and c) show exemplarily the overall prediction of the tangent stiffness K_T . These values are used to estimate the accumulated maximum force, presented in Fig. 4 b) and d). For additional information the reader is referred to (Müller and Taras 2022 a), Müller and Taras 2022 b), Müller and Taras 2022 c)).

7. DNN-DSM Implementation and Initial Results

7.1 Implementation

The general implementation is based on the generic definition of the direct stiffness method (DSM) for beam elements. The initial problem is derived from Eq.(6).

$$F_{loc} = K_{e,loc} \cdot u_{loc} \quad (7)$$

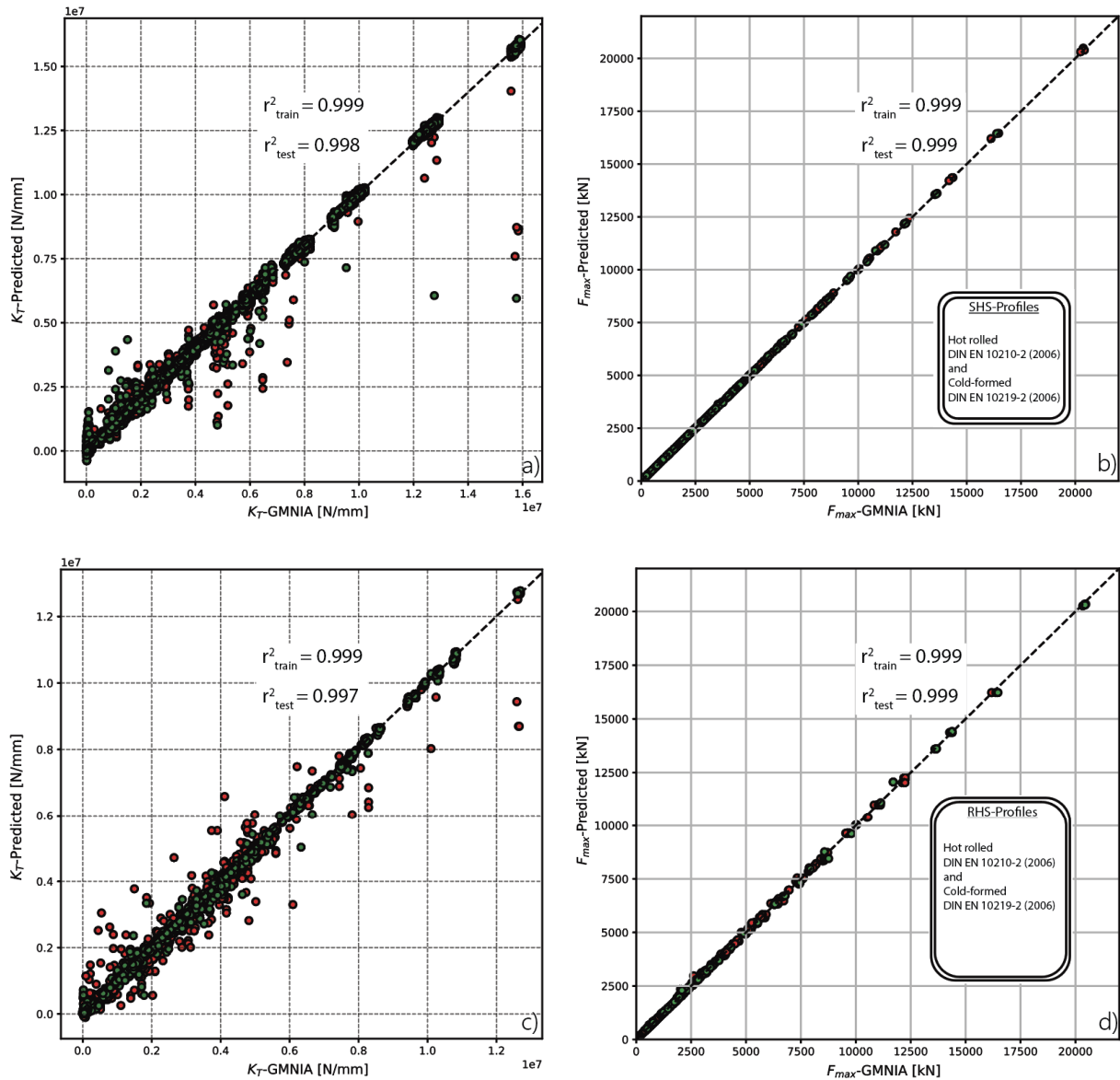


Figure 4: a) Simulation ($K_{T-GMNIA}$) vs. prediction ($K_{T-Predicted}$) for SHS profiles; b) Simulation ($F_{max-GMNIA}$) vs. prediction ($F_{max-Predicted}$) for SHS profiles; c) Simulation ($K_{T-GMNIA}$) vs. prediction ($K_{T-Predicted}$) for RHS profiles; d) Simulation ($F_{max-GMNIA}$) vs. prediction ($F_{max-Predicted}$) for RHS profiles

With the elastic local truss stiffness $K_{e,loc}$ as follows:

$$K_{e,loc} = \frac{EA}{L} \cdot \begin{bmatrix} 1 & 0 & -1 & 0 \\ 0 & 0 & 0 & 0 \\ -1 & 0 & 1 & 0 \\ 0 & 0 & 0 & 0 \end{bmatrix} \quad (8)$$

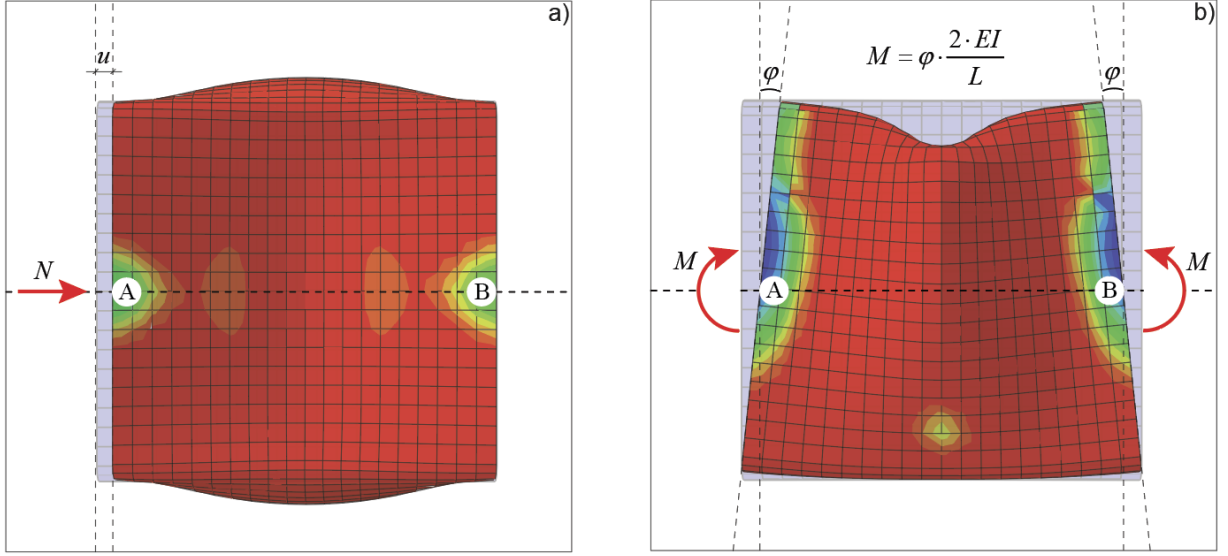


Figure 5: Deformation and rotation definition for a) the case of pure compression; b) the case of pure bending

After forming a global system of equations $F_{sys} = K_{e,sys} \cdot u_{sys}$, the nodal displacements u_{sys} due to a given load F_{sys} are determined by taking the inverse of system stiffness:

$$u_{sys} = K_{e,sys}^{-1} \cdot F_{sys} \quad (9)$$

The DNN-DSM makes use of this implementation to predict a local nonlinear tangent stiffness matrix $K_{T,loc,pred}^i$ according to a given nodal deformation u_{loc}^i , applied through incremental deformation steps $\Delta u_{loc}^{i+1} = u_{loc}^{i+1} - u_{loc}^i$ on the local element level. In this consideration $f(X)$ is the prediction done by the DNN model. X is the 2D matrix describing the data set $X \in \mathbb{R}^{n \times m}$ corresponding to the used model features. The accumulated displacement vector $u_{loc} \in X$ is part of the used features space. Eq.(10) describes the calculation of the incrementally derived force $\Delta F_{loc,pred}^{i+1}$.

$$\Delta F_{loc,pred}^{i+1} = f\left(X\left(u_{loc}^{i+1}\right)\right) \cdot K_{e,loc} \cdot \Delta u_{loc}^{i+1} \quad (10)$$

In more general terms, the calculated absolute force $F_{loc,pred}^{i+1}$ at any given local element displacement u_{loc}^{i+1} can be described by the following equation.

$$F_{loc,pred}^{i+1} = \sum_{i=0}^m f\left(X\left(u_{loc}^{i+1}\right)\right) \cdot K_{e,loc} \cdot \Delta u_{loc}^{i+1} \quad (11)$$

The implementation of the beam element follows a similar approach by modifying the beam stiffness matrix according to a given rotation φ , which is considered as one of the features for the DNN model prediction. The corresponding definition of the rotation φ for an element is stated in

Fig. 5 b). An equal constant rotation at both ends is assumed within the framework of the presented method. Therefore, the resulting constant moment along the element length L is defined through Eq.(12). Note that this formulation is assumed only in the elastic range.

$$M = \varphi \cdot \frac{2EI}{L} \quad (12)$$

The general notation for the elastic local beam element stiffness is represented by Eq.(13). Further, the stiffness component for constant bending can be factored out to be more in the line with the implementation idea.

$$K_{e,beam} = \begin{bmatrix} 12 \frac{EI}{L^3} & 6 \frac{EI}{L^2} & -12 \frac{EI}{L^3} & 6 \frac{EI}{L^2} \\ 6 \frac{EI}{L^2} & 4 \frac{EI}{L} & -6 \frac{EI}{L^2} & 2 \frac{EI}{L} \\ -12 \frac{EI}{L^3} & -6 \frac{EI}{L^2} & 12 \frac{EI}{L^3} & -6 \frac{EI}{L^2} \\ 6 \frac{EI}{L^2} & 2 \frac{EI}{L} & -6 \frac{EI}{L^2} & 4 \frac{EI}{L} \end{bmatrix} = \frac{2EI}{L} \begin{bmatrix} \frac{6}{L^2} & \frac{3}{L} & -\frac{6}{L^2} & \frac{3}{L} \\ \frac{3}{L} & 2 & -\frac{3}{L} & 1 \\ -\frac{6}{L^2} & -\frac{3}{L} & \frac{6}{L^2} & -\frac{3}{L} \\ \frac{3}{L} & 1 & -\frac{3}{L} & 2 \end{bmatrix} \quad (13)$$

Again, the predicted incremental force vector is written as follows, following the approach within the truss implementation from Eq. (10). Note that $\varphi_{beam,mean}^{i+1}$ is the mean between the rotation at node A and B from Fig. 5 b).

$$\begin{bmatrix} \Delta V_{beam,pred(AB)}^{i+1} \\ \Delta M_{beam,pred(AB)}^{i+1} \\ \Delta V_{beam,pred(BA)}^{i+1} \\ \Delta M_{beam,pred(BA)}^{i+1} \end{bmatrix} = f \left(X \left(\varphi_{beam,mean}^{i+1} \right) \right) \cdot \frac{2EI}{L} \begin{bmatrix} \frac{6}{L^2} & \frac{3}{L} & -\frac{6}{L^2} & \frac{3}{L} \\ \frac{3}{L} & 2 & -\frac{3}{L} & 1 \\ -\frac{6}{L^2} & -\frac{3}{L} & \frac{6}{L^2} & -\frac{3}{L} \\ \frac{3}{L} & 1 & -\frac{3}{L} & 2 \end{bmatrix} \cdot \begin{bmatrix} \Delta v_{beam(AB)}^{i+1} \\ \Delta \varphi_{beam(AB)}^{i+1} \\ \Delta v_{beam(BA)}^{i+1} \\ \Delta \varphi_{beam(BA)}^{i+1} \end{bmatrix} \quad (12)$$

7.2 Step Size Influence

The incremental step size, equivalent to the incremental nodal deformation $\Delta u_{loc}^{i+1} = u_{loc}^{i+1} - u_{loc}^i$, is discussed within Fig. 6 regarding on its influence on the prediction with respect to the GMNIA simulation. The x-axis is always showing the nodal displacement, the y-axis the corresponding force at each increment. The ground truth is given by the GMNIA simulation, here shown as a black line. The green line is the DNN model prediction in the pre-buckling range, using exactly the same deformation steps as extracted from the Abaqus FE shell calculation, i.e., the data that the DNN model was trained on. The dotted grey lines represent the DNN-DSM calculation, using

a different amount of incremental deformations Δu_{loc} until reaching a defined u_{loc} . All diagrams show exclusively the pre-buckling deformation range.

A clear influence can be drawn from the size of the incremental deformation. With decreasing step size the accuracy of the prediction start to decrease. This is illustrated through Fig. 6 a), b) and c), where the step size decreases from 20 to 4. This can be explained through the following steps. The prediction for $K_{T,loc}^{i+1}$ is done by using an absolute deformation u_{loc}^{i+1} at a current deformation of u_{loc}^i . Therefore, at points with stiffness jumps, i.e. a kink in the load-deformation curve, predictions with too large step sizes may lose stiffness too early.

To avoid this problem, a step size optimizer can be introduced, in which the step size is dynamically adjusted dependent on an error definition from the residuum. In the context of Fig. 6 d) the step size was halved if the calculated residuum is higher than a predefined threshold value. This automatically leads to an accumulation of calculations in areas with larger stiffness changes and thus an increase in computational effort. Nevertheless, this strategy enables a save computational propagation with a small number of steps and still a high prediction accuracy.

7.3 DNN-DSM Model Evaluation

Initial investigations presented herein focus exemplary on the influence of modelling approaches within the DNN-DSM implementation and comparisons with 4 point bending tests from literature (Wang et al. 2016).

Fig. 7 and 8 illustrate GMNIA simulations with different ascending lengths, always composed of a multiple of the buckling length ($L = \max(H, W)$) being the maximum of either the profile height or the width.

Fig. 7 shows an SHS 300×6.3, S690 profile with the length of 600 mm and 900 mm. The GMNIA Abaqus simulations shows in the case of the 600mm member a constant buckling over the whole length forming two main buckling fields. Thus, the deformation of the whole member is more pronounced in the post-buckling region. A similar behavior can be achieved with DNN-DSM model 1 with equivalent imperfection amplitudes $B/200$. In addition, model 2 uses two different imperfection amplitudes, $B/200$ and $B/300$, in order to achieve buckling in only one buckling field. This leads, in particular, to a larger drop of the load-deformation curve within the post-buckling range. This behaviour is somehow logical, since the deformations are not distributed over the whole member length, but are concentrated in one field.

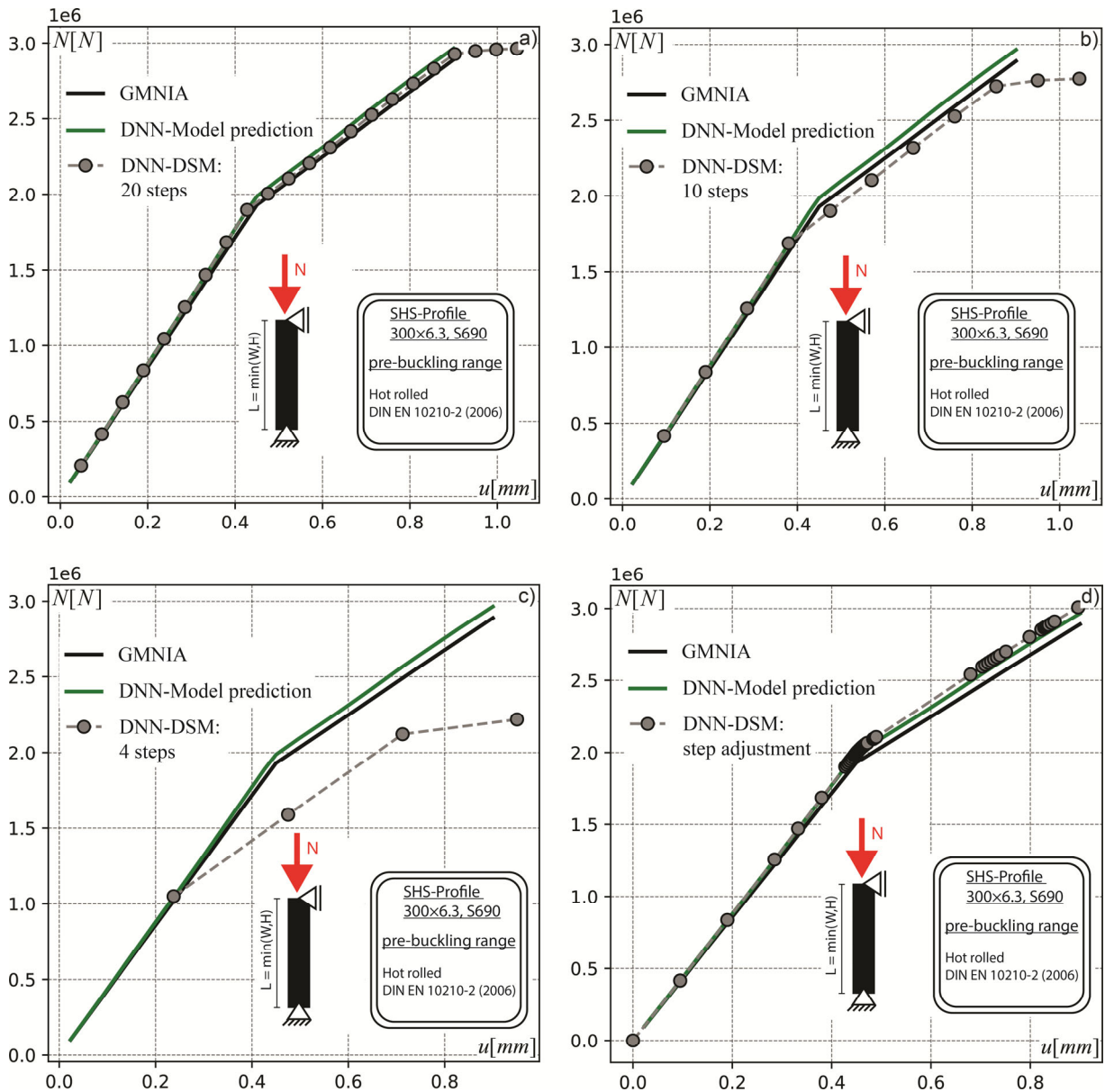


Figure 6: Influence of the amount of steps on the prediction accuracy a) 20 steps; b) 10 steps; c) 4 steps; d) dynamic step optimization

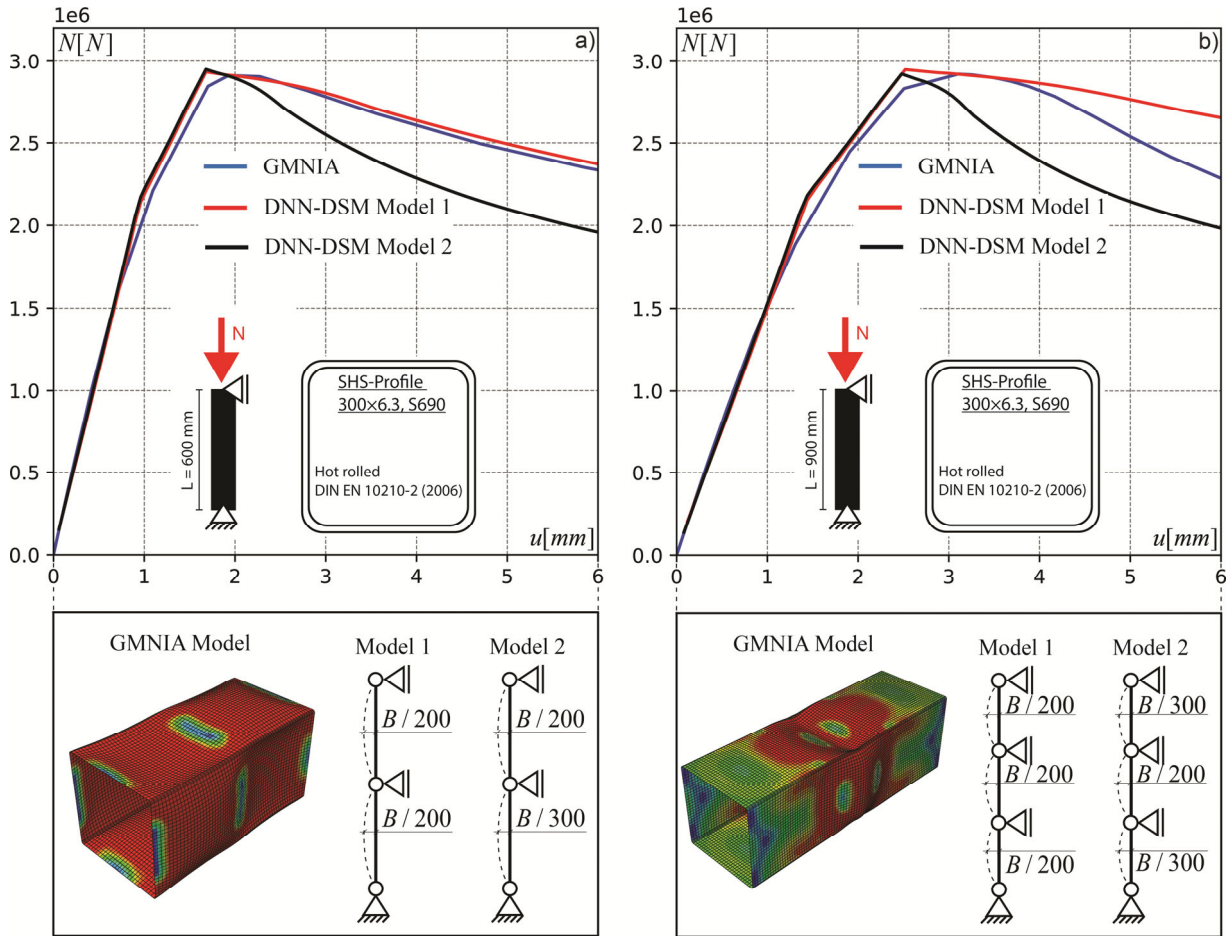


Figure 7: Comparison between GMNIA simulations and two DNN-DSM model approaches a) member length equal to 600mm; b) member length equal to 900mm

Fig. 7 b) show the results for the member length of 900 mm. In contrast to Fig. 7a), buckling arises exclusively in one field in the middle of the member, leading to a steeper drop of the load-deformation curve in the post-buckling range. DNN-DSM model 2 reproduces the simulated GMNIA behavior nicely, although slightly phase shifted with respect to the maximum force.

A similar behaviour as shown in Fig. 7 a) for $L = 600$ mm can be observed from Fig. 8 a) $L = 1200$ mm. Again, buckling is introduced over the whole length of the member, leading to a pronounced post-buckling behaviour. This behaviour is best reproduced by DNN-DSM model 1, assuming equivalent imperfections amplitudes for each predicted element. Fig. 8 b) indicates the results for the member length of 1500 mm. Two buckles, at the top and the bottom occurred within the GMNIA simulation. According to this, 3 different DNN-DSM models were implemented to observe the overall load-displacement prediction. Model 1 uses an equivalent imperfection amplitude with $B/200$. Model 2 uses two imperfection amplitudes, $B/200$ and $B/300$ in order to force the model to buckle exclusively in one field. Model 3 uses the same imperfection approach as Model 2, with the difference that buckling is introduced in the upper and lower element only.

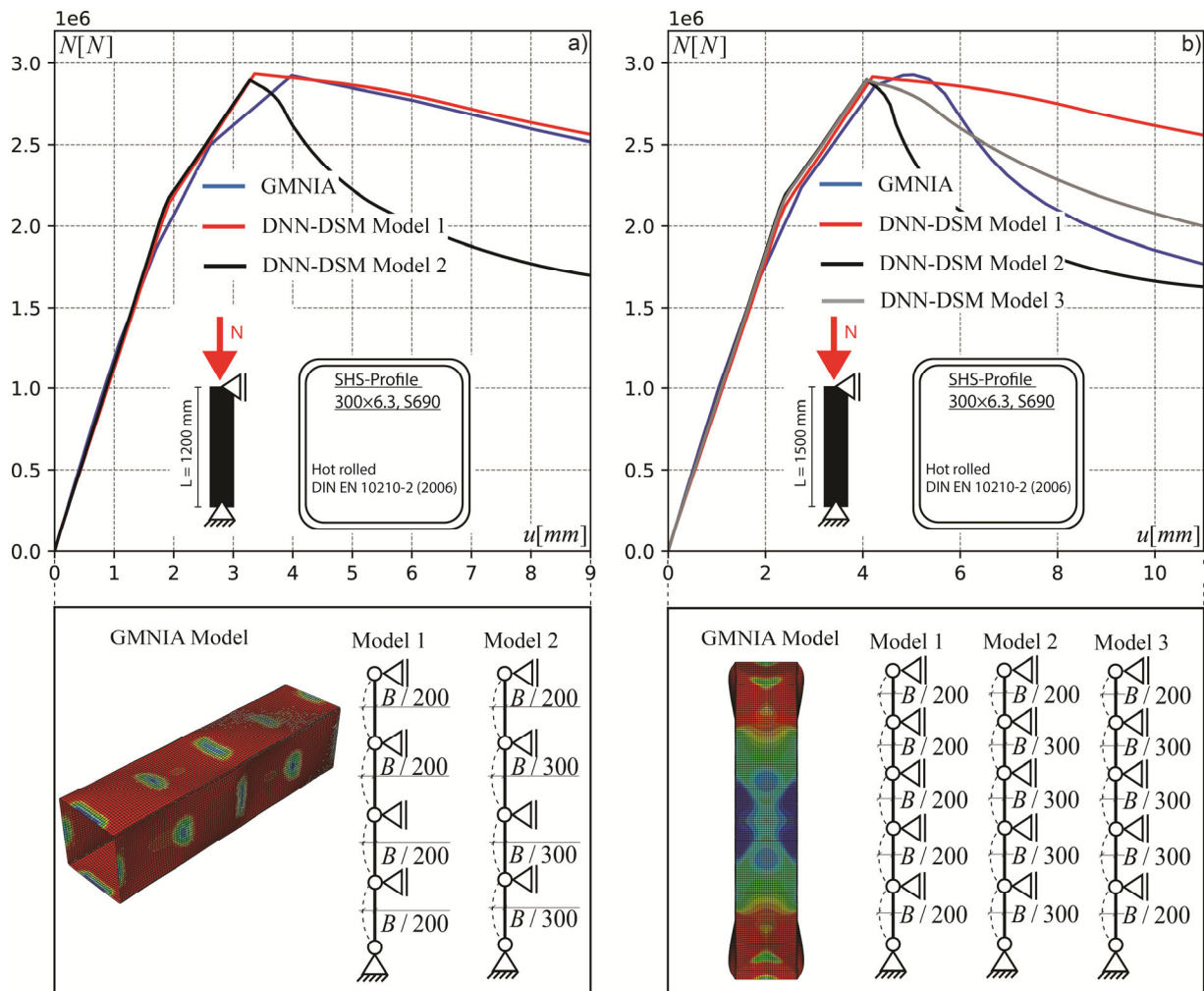


Figure 8: Comparison between GMNIA simulations and two DNN-DSM model approaches a) member length equal to 1200mm; b) member length equal to 1500mm

According to the overall prediction of the pre- and post-buckling range DNN-Model 2 (buckling in one element) leads to load-deformation curve similar to one produced by GMNIA. Again, a displacement shift at the point of the maximum force is identified. This behavior is exclusively attributable to the GMNIA Abaqus simulations simplified in the first step, where a large solver step time was initially selected in order to speed up the calculation and prove a basic method feasibility. Evaluations with more refined load-displacement predictions are under way and will be presented in future publications.

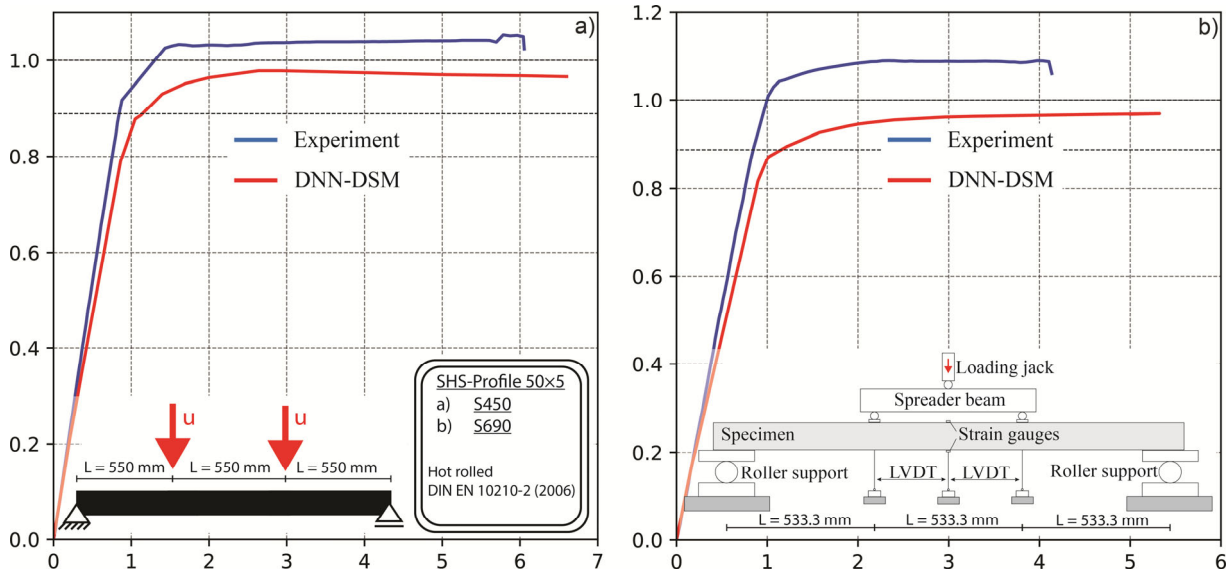


Figure 9: 4 point bending tests on hot-finished hollow sections by (Wang et al. 2016), here for an SHS50×5 profile a) S450; b) S690

Fig. 9 presents a comparison between 4 point bending tests performed by (Wang et. al 2016) and own DNN-DSM beam predictions. The experimental set up is exemplary presented within Fig. 9 b). The loading was introduced in the third points of the beam. The length of the third correspond to 533.3 mm in the experiment. Further information shall be taken from (Wang et al. 2016). The DNN-DSM model is depicted in Fig. 9 a). The third lengths deviate slightly from the lengths in the experimental result, since the current model implementation is based on fixed local lengths, linked to the maximum value of the cross-section height or width, here being always a multiple of 50 mm.

The diagrams show a normalized representation of the moment-rotation output, normalized by the plastic rotation and moment in the x- and y-axis, respectively. The DNN-DSM model results are in both representations of Fig. 9 below the experimentally derived curves, although showing a similar overall behavior in the elastic and plastic range. The differences are attributed to simplifications within the current model accuracy, which in this study consisted of a simplified bilinear material model with a perfectly plastic plateau assumed for all material grades, Abaqus solver settings leading bigger step sizes within the calculation and current implementation boundaries constrained by fixed buckling lengths.

8. Conclusions and Outlook

The presented paper describes first findings and results towards a novel method (DNN-DSM), combining the computational advantages of beam-element models with the accuracy of numerical shell-element based simulations. The connection is made by using predictive models based on the concepts and techniques from machine and deep learning, trained and tested on data sets derived from a pool of Abaqus shell element simulations. Preliminary investigations on feature engineering, i.e. data transformation, data splitting and investigations on feature importance, were presented in previous publications (Müller and Taras 2022a), Müller and Taras 2022b), Müller and Taras 2022c)) and therefore only presented informatively.

Initial implementation results with different modelling approaches of the DNN-DSM are presented for the load case of pure compression and pure bending, respectively. The overall results fit the GMNIA simulations as well experimental results, providing the framework for additional refinements throughout the upcoming research. The current work focuses on modeling approaches, 2nd order instability effects and the extension of the method to frame structures.

References

- Abaqus. Reference manual, version 6.16. (2016). *Simulia, Dassault Systèmes*. France.
- AISC 360-16. (2016). "Specification for structural steel building." *American Institute of Steel Constructions*, Chicago.
- Baker, J. F. and Roderick, J. W. (1938) "An experimental Investigation of the Strength of Seven Portal Frames." First interim Report, Research Committee of the Institute of Welding, Transactions of the Institute of Welding, Vol 1, No4.
- Baker, J. F. and Roderick, J. W. (1940) "Further tests on Beams and Portals." Second interim Report, Research Committee of the Institute of Welding, Transactions of the Institute of Welding, Vol 3, No2.
- Baker, J. F., Horne, M. R., Heyman, J. (1956) "The Steel Skeleton, Volume 2: Plastic Behaviour and Design." *Cambridge University Press*, Cambridge, England.
- Breiman, L. (2001). "Random Forest." *Machine Learning*, 45, 5-32.
- Chen, T., Guestrin, C. (2016). "XGBoost: A scalable tree boosting system." *In: Proc ACM SIGKDD Int Conf Knowl Discov Data Min*, 785-94.
- DIN EN 1993-1-1. (2006). "Eurocode 3. Design of steel structures – Part 1-1: General rules and rules for buildings." *CEN – European Committee for Standardization*, Brussels.
- DIN EN 1993-1-5. (2006). "Eurocode 3. Design of steel structures – Part 1-5: Plated structural elements." *CEN – European Committee for Standardization*, Brussels.
- DIN EN 10210-2. German version EN 10210-2: (2006). "Hot finished structural hollow sections of non-alloy and fine grain steels – Part 2: Tolerance, dimensions and sectional properties."
- DIN EN 10219-2. German version EN 10219-2: (2006). "Cold formed welded structural hollow sections of non-alloy and fine grain steels – Part 2: Tolerances, dimensions and sectional properties."
- Driscoll, G. C., Beedle, L. S., Galambos, T. V., Lu, L. W., Fisher, J. W., Ostapenko, A., Daniels, J. H. (1965) "Plastic design of multi-story frames-Lecture Notes." *Lehigh University*, Bethlehem, Pennsylvania, USA.
- Ewing, J. A. (1899). "The Strength of Materials." Cambridge.
- Fieber, A.C. (2019). "Structural Steel Design using Advanced Analysis with Strain Limits." *Ph.D. Thesis, Department of Civil and Environmental Engineering*, Imperial College London.
- Frochte, J. (2018). „Maschinelles Lernen. Grundlagen und Algorithmen in Python.“ Carl Hanser Verlag München.
- Fritsche, J. (1930) "Die Tragfähigkeit von Balken aus Stahl mit Berücksichtigung des plastischen Verformungsvermögens." *Der Bauingenieur 11*, pp. 851-855, 873-874 & 888-893.
- Galambos, T. V. (1968) "Structural Members and Frames." *Prentice-Hall Series in Structural Analysis and Design* (W. J. Hall, editor), Prentice-Hall, London, U.K..
- Gardner, L. (2008). "The continuous strength method." *Proceedings of the Institution of Civil Engineers – Structures and Buildings*, 161(3), 127-133.
- Girkmann, K. (1931) "Bemessung von Rahmentragwerken unter Zugrundelegung eines ideal plastischen Stahles." *in: Sitzungsberichte der Akademie der Wissenschaften in Wien, math-naturw. Klasse Abt. IIa*, 140, Band, H. 9u 10, Wien, 1931.

- Gruning, M. (1926) "Die Tragfähigkeit statisch unbestimmter Tragwerke aus Stahl bei beliebig häufig Wiederholter Belastung." *Berlin: Springer*.
- Kazinczy, G. (1914) "Trials with fixed-end beams." *Betonszemle*, Issue 2, pp. 68-71, 83-87&101-104.
- Kist, N. C. (1920) "Die Zähigkeit des Materials als Grundlage für die Berechnung von Brücken, Hochbauten und ähnlichen Konstruktionen aus Flusseisen." *Der Eisenbau 11*, No. 23, pp. 425-428.
- Maier-Leibnitz, H. (1928) "Beitrag zur Frage der tatsächlichen Tragfähigkeit einfacher und durchlaufender Balken-träger aus Baustahl St 37 und Holz." *Die Bautechnik 6*, pp. 11-14 & 27-31.
- Maier-Leibnitz, H. (1929) "Versuche mit eingespannten Balken von I-Form aus Baustahl St 37." *Die Bautechnik 7*, pp. 20 & 313-318.
- Massonnet, C. (1976) "Die europäischen Empfehlungen (EKS) für die plastische Bemessung von Stahltragwerken." *Acier-Stahl-Steel 32*, pp.146-156.
- Meng, X., Toffolon, A., Gardner, L., Taras, A. (2019). "The generalised slenderness-based resistance method for the design of CHS and EHS." *Steel Construction*, Vol. 12, Issue 4, Wiley.
- Meyer, E. (1908) "Die Berechnung der Durchbiegung von Stäben deren Material dem Hook'schen Gesetze nicht folgt." *Zeitschrift des Vereines Deutscher Ingenieure*, 52(5), p.167.
- Müller, A., Taras A. (2019). "On the post-buckling rotational capacity of squared hollow sections in uniform bending. An initial study on the impact of initial imperfections on deformation paths." *Steel Construction – Design and Research 12*, No. 3 (8).
- Müller, A., Taras A. (2022a). "Prediction of the load-displacement and local buckling behavior of hollow structural sections using Deep Neural Networks (DNN)." *Proceedings of SSRC 2019*, Denver.
- Müller, A.; Taras, A. (2022b) „Prediction of the local buckling strength and load-displacement behaviour of SHS and RHS members using Deep Neural Networks (DNN) – Introduction to the Deep Neural Network Direct Stiffness Method (DNN-DSM).“ *Steel Construction 15*, Hollow Sections, pp. 78–90. <https://doi.org/10.1002/stco.202100047>
- Müller, A., Taras A., Kraus, A.K., (2022c). "Scientific Machine and Deep Learning Investigations of the Local Buckling Behaviour of Hollow Sections." *Proceedings of SDSS 2022*, Aveiro, Portugal.
- Schaim, J. H. (1930) "Der durchlaufende Trager unter Berücksichtigung der Plastizität." *Stahlbau 3*, pp. 13-15, 1930.
- Toffolon, A., Müller, A., Nico, I. Taras, A. (2019a). "Experimental and numerical analysis of the local and interactive buckling behaviour of hollow sections." *Proceedings of SDSS 2019*, Prague.
- Toffolon A., Meng X., Taras A., Gardner L. (2019b). "The generalised slenderness-based resistance method for the design of SHS and RHS." *Steel Construction*, Vol. 12, Issue 4, Wiley.
- Toffolon, A., Taras, A. (2019c). "Development of an OIC-Type local buckling design approach for cold-formed unstiffened and groove-stiffened hollow sections." *Thin-Walled Structures*, 144 (6) Elsevier.
- Toffolon A., Taras A. (2019d) "Proposal of a design curve for the overall resistance of cold formed RHS and SHS members", *Conference Paper, Nordic Steel Conference 2019*, Copenhagen.
- Walport, F. (2019). "Design of steel and stainless Steel Structures by Advanced Inelastic Analysis." *Ph.D. Thesis, Department of Civil and Environmental Engineering*, Imperial College London.
- Wang, J., Afshan, S., Gkantou, M., Theofanous, M., Baniotopoulos, C., Gardner, L. (2016) "Flexural behaviour of hot-finished high strength steel square and rectangular hollow sections." *Journal of Constructional Steel Research*, vol. 121, pp. 97-109. <https://doi.org/10.1016/j.jcsr.2016.01.017>
- Yun, X., Gardner, L. (2017). "Stress-Strain curves for hot-rolled steels." *Journal of Constructional Steel Research 133* (6) 36-46.
- Yun, X., Gardner, L. (2018). "Description of stress-strain curves for cold-formed steels." *Construction and Building Material 189* (11) 527-538.